

Flow in the Low Specific Speed Centrifugal Pump with Circular Casing

Jun MATSUI*	Yokohama National Univ., Japan	jmat@mach.me.ynu.ac.jp
Junichi KUROKAWA	Yokohama National Univ., Japan	kuro@mach.me.ynu.ac.jp
Young-Do CHOI	Yokohama National Univ., Japan	ydchoi@mach.me.ynu.ac.jp
Kouichi NISHINO	Yokohama National Univ., Japan	nish@ynu.ac.jp

Key words: Turbomachinery, Centrifugal Pump, Low Specific Speed, Spiral Casing, Circular Casing

Abstract

The internal flow of a centrifugal pump with semi-open impeller, whose type-number is 0.244, is measured by PIV method and analyzed numerically. The head and efficiency of a pump that has a circular casing with a very small radius are almost same as those of the spiral casing. Even at the best efficiency point, the internal flow in the pump of circular casing is asymmetric. The flow goes out from the impeller only at the exhaust area of the casing. Also, there is a very strong unsteady flow near this area.

Introduction

When the specific speed or type-number is low, the efficiency of most centrifugal pumps becomes lower (Ref 1). The authors have studied on the performance of centrifugal pump for the low specific speed, and have made clear the effects of impeller and casing parameters on the performance (Ref 2, 3) near $n_s = 60$ [m, m³/min, min⁻¹] (the type-number $k=0.14$). The increase of leak and increase of roughness of impeller disc can increase efficiency (Ref 4). Also, semi-open type impeller may be suitable because of their good stability (Ref 5), comparing with the closed type impeller (Ref 6, 7).

In most of these studies, we use a spiral casing, so next we try to use circular casings, hoping that we can easily get very smooth surface by grinding. In the region of low specific speed, the friction loss becomes very large, so the circular casing has an advantage. For $k < 0.146$, the authors got good performance using the circular casing (Ref 8).

In this study, we try the circular casing with very small radius for type number $k=0.244$ (the specific number $n_s=100$ [m, m³/min, min⁻¹]). The performance becomes almost same as the spiral casing. To investigate this reason, we analyze the internal flow in this pump, both by CFD method and by experimental one.

Experimental Apparatus and Method

The experimental system and the expansion of the test section are shown in Figure 1 . The channel between inlet of the impeller and outlet of the casing is made as a two-dimensional

configuration between two pieces of flat plates. The front wall and side walls of the casing in the test section are made of transparent acrylic resin, for the visualization and the image velocimetry in the pump. Also, the shape of the casing is easily changed and modified.

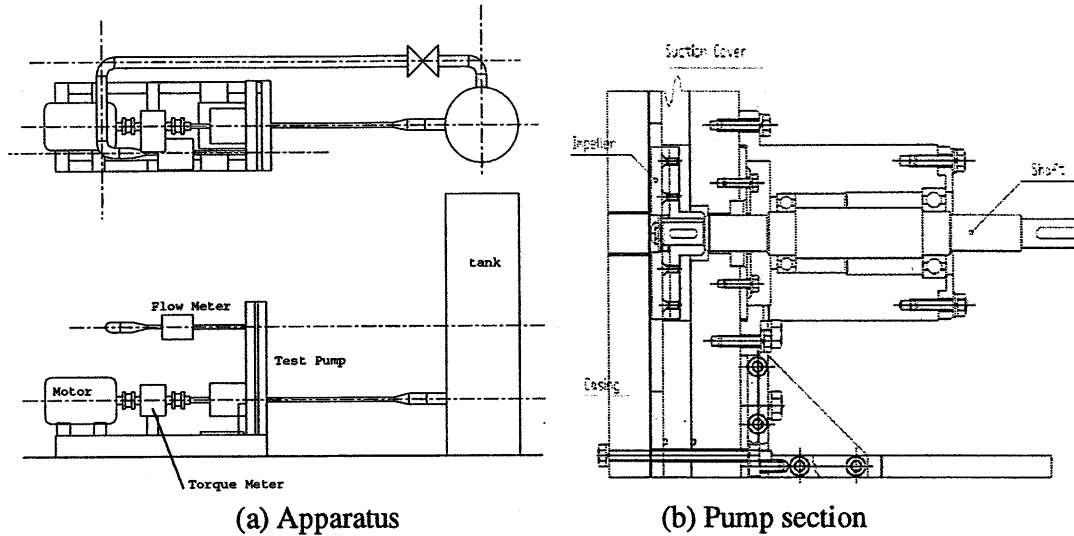


Figure 1 Experimental apparatus

Figure 2(a) shows the schematic view of the test impeller. This impeller is the semi-open type, whose outlet angle of the blade is $\beta_2 = 30$ degree. The tip clearance $c/b_2 = 0.125$, while b_2 is 8[mm]. The rotational speed of the axis is $n=900$ [rpm].

The shapes of test casing are shown in Figure 2 (b). The cross section area at the discharge throat A_3 of the casing is $A_3/A_2 = 0.056$ for all casings. These casings are designed as the type-number k becomes 0.244 at the matching point between impeller and casing.

The spiral casing has a logarithmic radius, because the depth of the casing is constant. After the discharge throat, two types of channel are used. One channel is expanded with $2\theta_v = 8$ deg. The other channel has a straight shape. The inner wall of each channel is polished well. In the Figure 2(b), the shape of type A that has a straight channel is shown. Also, the type A' casing has an expanded diffuser channel. The outer radius r_3 of circular casings has the various radius that are $R = r_3/r_2 = 1.03, 1.15, 1.3, 1.5$.

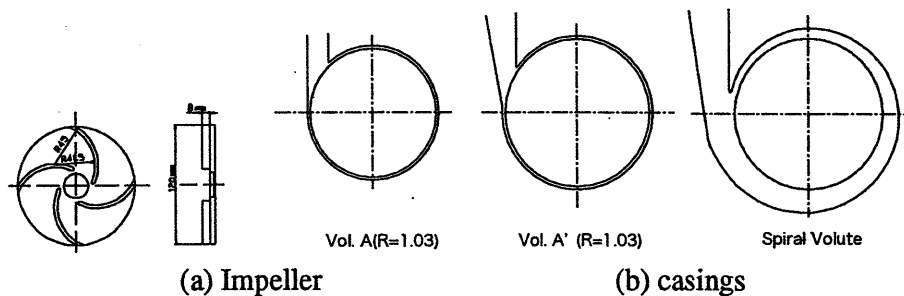


Figure 2 Impeller and casings

The internal velocity field near the tongue area is measured by PIV method. A double-pulsed Nd:YAG laser sheet (20 mJ) is used as a source of illumination. The thickness of the light sheet is fixed to 0.5 mm. A CCD camera whose resolution is 1300 x 1030 pixel takes the image of the flow field from the direction perpendicular to a plane of light sheet. The intervals

of the laser pulses are set to $100 \mu s$. Particles of nylon 12 whose diameter is about $30 \mu m$ are used as tracers.

Three separate planes in the direction perpendicular to the impeller axis are measured: near the suction cover ($z/b = 0.8$), middle passage width ($z/b = 0.5$), and near the main shroud ($z/b = 0.2$), while z is a wall-normal distance from the shroud side wall, and b is an impeller passage height (9mm). An example of the photo taken by this PIV system is shown in Fig. 3. Though there are shadows made by impeller blade and casing tongue, the exhaust area of the casing is taken very clearly. So we'll discuss on this area for the result of PIV.

A triggering signal is captured from the shaft of the pump, so that the PIV images in which the impeller blade is at the same position is collected and averaged.

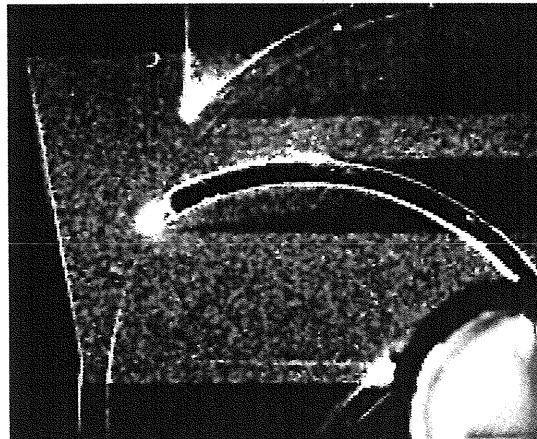


Figure 3 Example of PIV photo at $\zeta=75[\text{deg}]$

Numerical method

Unsteady numerical simulations are enforced using the commercial software, CFX-5.7. The calculating area is divided into four parts, the suction pipe, exhaust pipe, impeller, and casing. The total node number is about 1300,000, in all cases. While the result is compared with the grid of smaller and larger node number, the grid dependency was not found. The total analyzing grid and its magnification of tongue area are shown in Fig. 6. The suction pipe grid and impeller grid are combined by the transient rotor-stator method. The same method is used between the impeller and casing. The SST turbulent model is used.

At the inlet edge of the suction pipe, the average velocity value is given as the boundary condition. At the outlet edge of the exhaust pipe, the constant pressure is set. We confirm that the time-averaged head calculated by the CFD simulation agrees very well with the experimental result, both in the case of spiral casing and circular casing, as shown in the Fig. 5. Also, the calculated pressure distribution along the casing wall agrees well with the experimental results.

Results and discussions

Performance of the circular casing

The performance curves with various radius of the circular casings are shown in Fig.6 (a). The casing type A,B,C, and D have different outer radius, r_3 . In the case of type A, whose radius $R = r_3/r_2 = 1.03$, the discharge quantity at the best efficiency point (BEP) is $Q = 1.77[\text{m}^3/\text{h}]$,

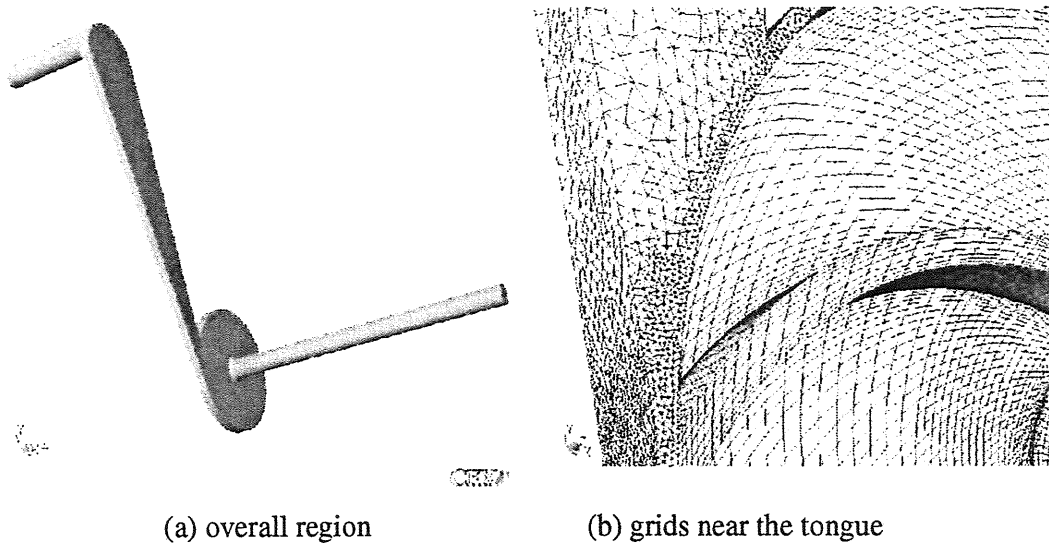


Figure 4 Calculating grid for the CFD analysis.

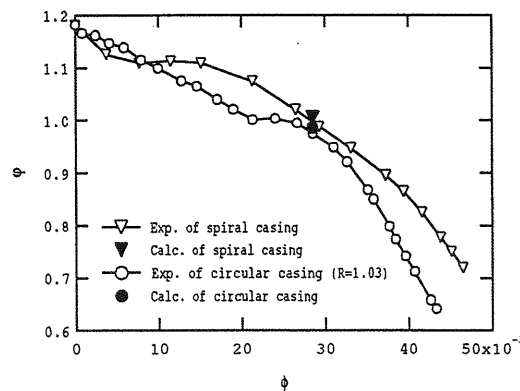


Figure 5 Performance by experiments and by CFD.

its discharge coefficient is 0.0293, the total head is $H=1.52$ [m]. The type-number at the best efficiency point is $k_{BEP} = 0.275$, that is a little higher than the designed value, 0.244.

As the increase of the outer radius R , the head is reduced, and at the smallest R , type A, it becomes highest. The power coefficient τ is not changed much, the type A casing shows the best efficiency in these casings. The agreement of the power coefficients indicates that the loss in the casing is the main reason of these differences of the head.

The performance of the spiral casing is compared with that of the circular casing A and A' in Fig. 6 (b).

The spiral casing shows the higher head coefficient ψ in almost all range of the discharge coefficient. The circular casing of type A' shows the almost same head and efficiency near the best efficiency point, but at the larger discharge coefficient, both head and efficiency are reduced. The efficiency of casing A is a little lower than that of type A'. So we compare the flow in the casing A' and that in the spiral casing, from here.

Transient velocity field (CFD)

Two examples of the velocity field in the spiral casing calculated by the CFD simulation are shown in Fig. 7. This figure is the velocity vectors on the cross section of $z/b = 0.5$. The

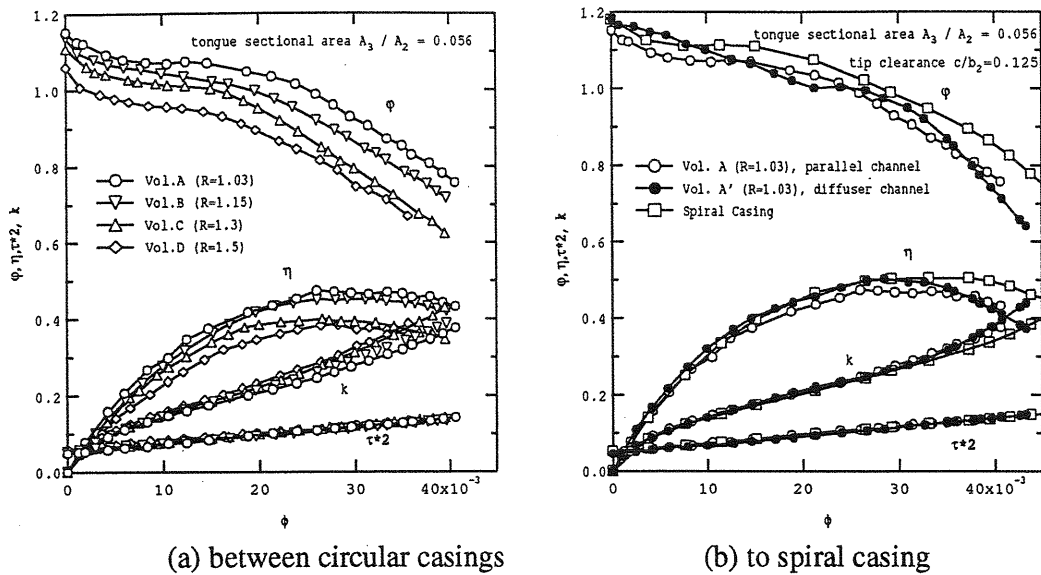


Figure 6 Performance change by casings (experimental results)

calculated discharge value is set at the best efficiency point in the experiment.

The angle ζ indicates the position of the impeller blade. When $\zeta=0$ degree, the center of the blade depth at r_2 is on the line between the center of the axis and tongue tip. Here the number of the impeller blade is four, so the next blade comes on that line when $\zeta=90$ degree.

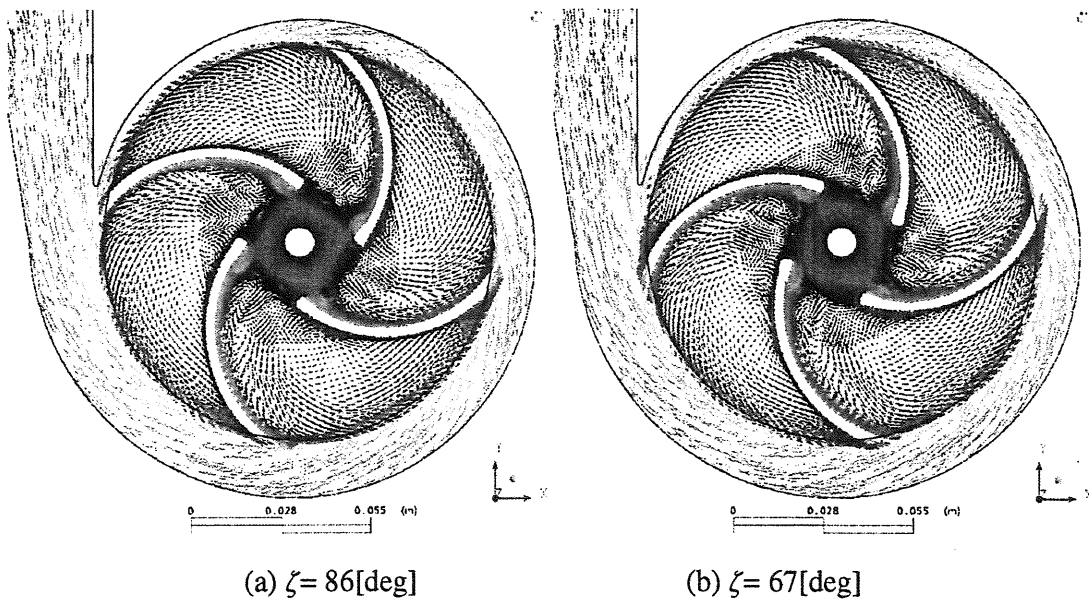


Figure 7 Transient velocity vectors in the spiral casing by CFD.

There are separated vortexes at the inlet of the impeller, and very strong secondary flow pulls the main stream to the suction side of the blade. This is a typical flow pattern in the low type number impeller. The flow pattern is not so changed between two figures, so the flow in the pump of spiral casing is near the steady flow, at its best efficiency point.

The flow in the pump of circular casing A' in Fig. 8 shows very different patterns from the above ones. There are large vortexes in the center of each impeller channels, except for the channel attached to the discharge throat region of the casing. The flow goes only at the throat

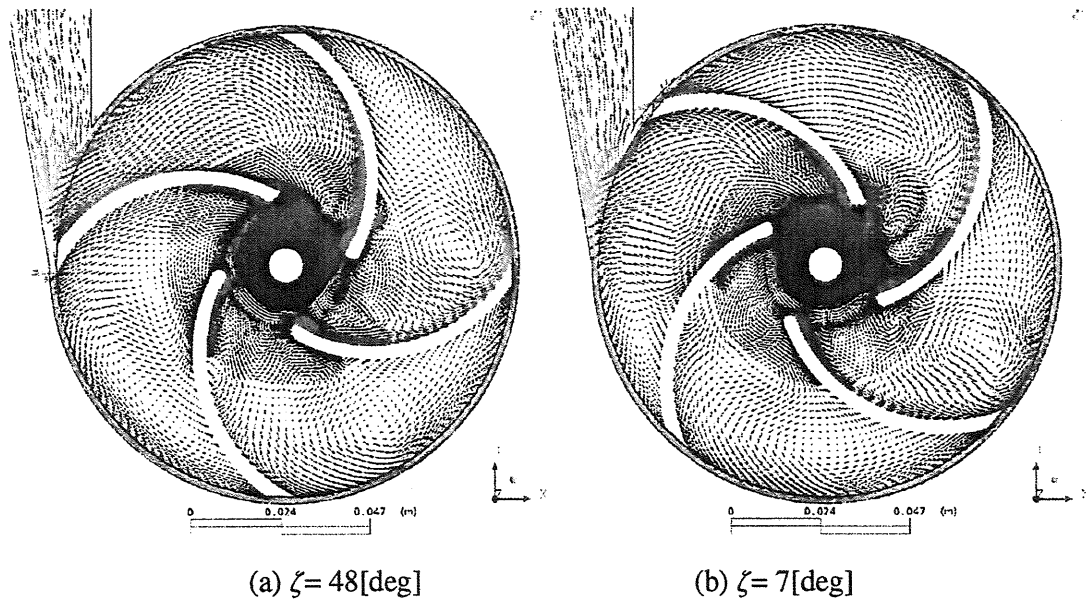


Figure 8 Transient velocity vectors in the circular casing A', by CFD.

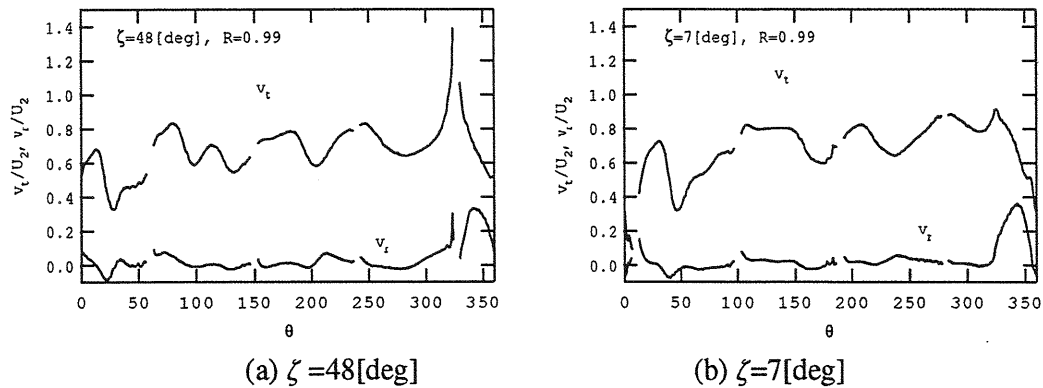


Figure 9 Transient velocity distribution in the circular casing A', by CFD

region and the flow does not go out from the impeller in other region. Even at the most efficient point, the flow in the pump is far from symmetric. Also the unsteadiness is much larger than that of spiral casing.

Figure 9 shows the velocity distribution at the impeller exit, $R = r/r_2 = 0.99$, for each case of Figure 8.

In the figure (a), when the blade is approaching to the discharge throat area of casing, the tangential velocity v_t becomes so large that it is more than the rotational speed of impeller U_2 . This fast flow is not found in the figure (b), so we can see that there is very strong unsteady flow in the impeller. Also, the radial velocity v_r becomes remarkable only at the discharge throat of the casing, from $\theta = 320$ degree to 360 degree. This tendency is not affected by the position of the blade, therefore, the flow in the impeller is strongly controlled by the casing.

Transient velocity distribution in the casing (PIV)

Figure 10 shows the transient velocity distribution at the discharge throat of the circular casing, measured by PIV method. The velocity data are collected on the plane $z/b = 0.5$ whose radius is $R = 1.01$, at the best efficiency discharge. The top of the tongue exists at $\theta = 0$. Figure

(a) shows the radial velocity divided by the rotational speed of impeller edge, U_2 . We can see the fast tangential flow at the pressure side of the blade, as the blade is moving from $\zeta=60, 75$, and 0 degree. From the angle $\theta=-40$ to 0 degree, that is the exhaust area of the casing, there almost always is an outward flow, which agrees with the CFD results. The tangential velocity v_t distribution indicates that near $\theta=35$ there always exists fast tangential flow about $v_t = 0.9U_2$. This is not so large as that in the CFD result at $R = 0.99$. During the flow goes into the casing from impeller, some mixing may make the distribution smoother.

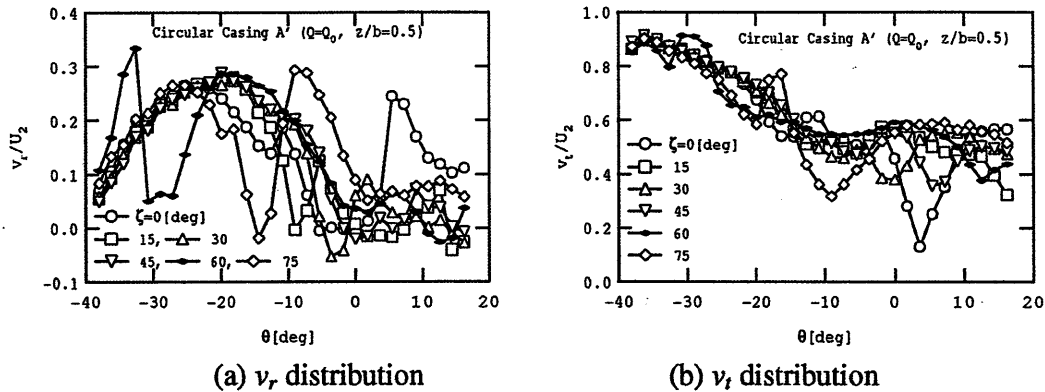


Figure 10 Transient velocity distribution by PIV measurement.

The velocity profile at each measuring planes, $z/b = 0.2, 0.5, 0.8$, is not so changed as shown in the Fig. 11. This is an example at $\zeta = 0$. Figure (a) shows the radial component of the velocity. On the plane $z/b=0.8$, there is a reversed flow near $\theta = 0$, where the impeller blade exists. At the partial discharge, $Q = 0.5Q_0$, the velocity profile is not so changed, while the value becomes smaller.

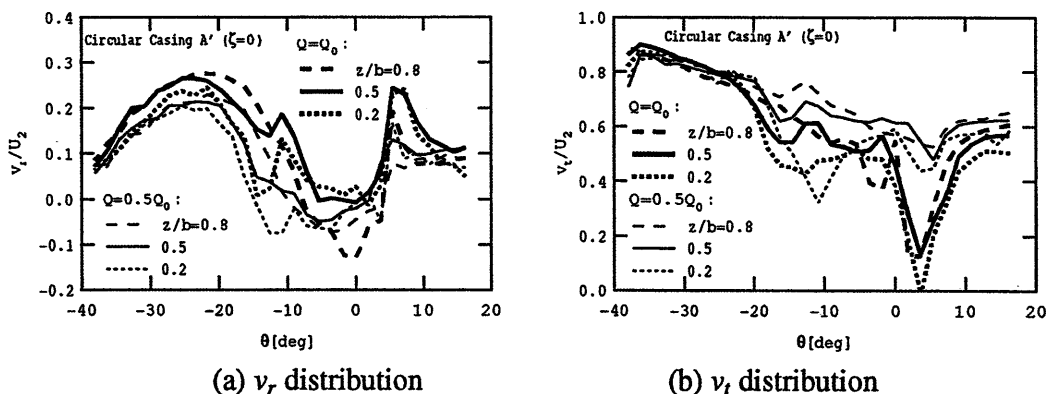


Figure 11 Transient velocity distribution by PIV measurement between z/b

The measured velocity distribution in the pump of spiral casing and circular casing is compared in Fig. 12. In the spiral casing, the radial velocity distribution becomes flat except just near the blade. The tangential velocity has the same tendency. These results are reproduced by the CFD analysis.

Time averaged velocity distribution (CFD)

The time-averaged velocity distribution calculated by CFD simulation is shown in Fig. 13. In the spiral casing, the radial velocity v_r is almost constant, with a small value. On the other hand,

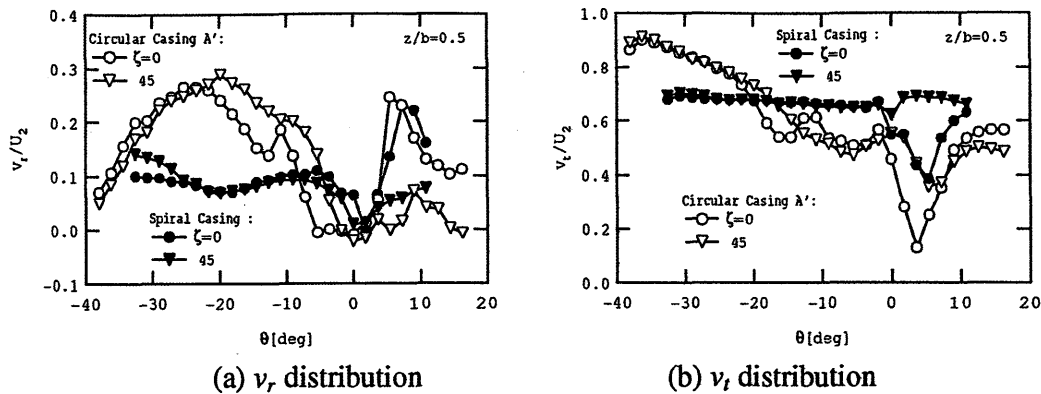


Figure 12 Comparison of Velocity distribution between in the spiral casing and in the circular casing.

in the circular casing, v_r is large only at the discharge throat of casing, and almost zero in other area.

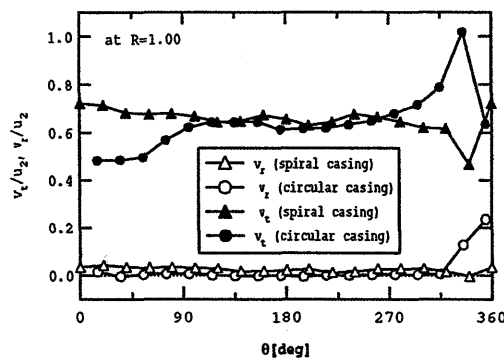


Figure 13 Averaged velocity distribution by CFD.

Pressure distribution (CFD)

Two examples of pressure distribution in the circular casing case, calculated by the CFD, are shown in Fig. 14. Near the pressure side of the blades, there are high pressure areas near the outer edge of the impeller, except for the blade near the exhaust of the casing. At this area, the pressure head seems to become the velocity head.

Though this circular casing has very narrow gap between the tongue and impeller, the pressure fluctuation is not so large according to the movement of blades. The very fast flow from impeller into the casing is not at the tongue but at the far side of the discharge throat area of the casing. So this flow does not collide directly to the tongue, and the pressure at the tongue is not so fluctuated.

Also in the figure (b), the pressure at tongue becomes large. This may be caused by the dynamic pressure of tangential flow in the casing, because at this blade position, the radial flow near the tongue is very small.

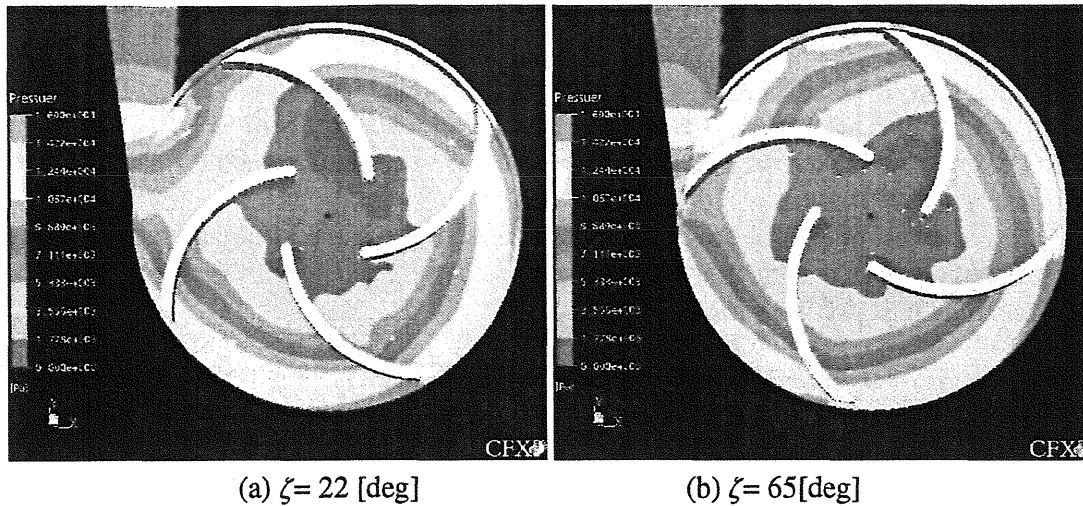


Figure 14 Pressure distribution by CFD

Axial thrust

The calculated radial thrust coefficient is shown in Fig. 15. The coefficient of thrust C_F is defined by the radial thrust force F_r as $C_F = F_r / (\frac{1}{2}\rho A_2 U_2^2)$. The figure (a) compares the thrust coefficient between the spiral and circular casing. While the spiral casing shows its minimum thrust at the best efficiency point $\phi = \phi_0$, the thrust of circular casing is in proportion to the ϕ . Though the flow is not symmetric in the circular casing pump, the order of the thrust force is same.

The radial thrust comes from two factors. One is the asymmetric distribution of pressure around the impeller. The other is a moment from the asymmetric flow from the impeller. In the ordinary case, the former is a major factor, because the velocity distribution around the impeller is near symmetric. But in the pump of circular casing, the flow is biased very much, so the latter becomes remarkable. The figure (b) shows these components of thrust in the circular casing. C_F is a total coefficient of the radial thrust. C_{FP} is a component of the thrust coefficient, that is summed from the pressure distribution around the impeller. This value can be gotten from the experimental data and CFD. These two C_{FP} are a little different, because this coefficient is very sensitive to the pressure. Only a small difference of pressure around the impeller causes relatively large difference of the C_{FP} . The difference $C_F - C_{FS}$ is a thrust force from the momentum term.

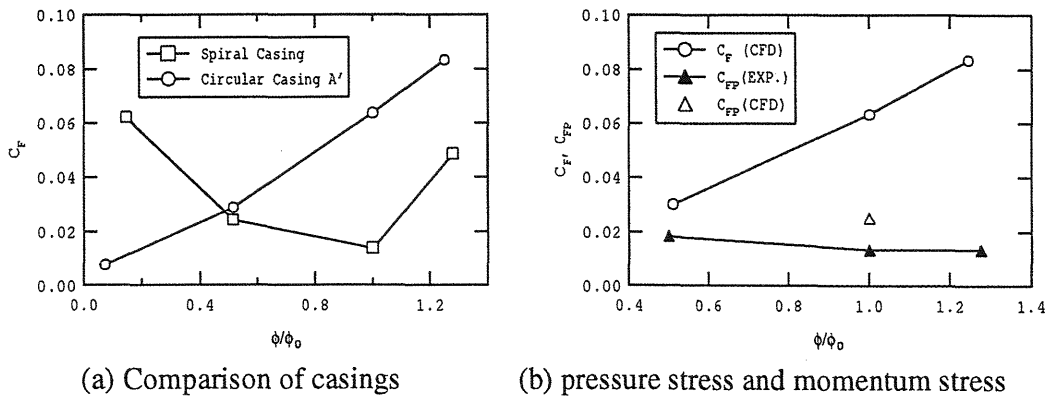


Figure 15 Radial thrust coefficient

Conclusion

The internal flow of a centrifugal pump with semi-open impeller, whose type-number is 0.244, is analyzed by PIV measurement and CFD. The pump with very small radius $R = 1.03$ of circular casing shows the best efficiency and head. Those values are almost same as that of spiral casing.

Even at the best efficiency point, the internal flow in the pump of circular casing is asymmetric. The flow goes out from the impeller only at the exhaust area of the casing. Also, there is a very strong unsteady flow near this area.

Reference

- Ref 1 Stepanoff, A. J., *Centrifugal and Axial Flow Pumps*, 2nd ed., p. 76, John Wiley and Sons. , 1957.
- Ref 2 Matsumoto, K., *et al.*, Performance of the Impeller for Very Low Specific Speed, *Turbomachinery (in Japanese)* , 25-7, pp. 337-345, 1997.
- Ref 3 Matsumoto, K., *et al.*, Study on Optimum Configuration of a Volute Pump of Very Low Specific Speed, *Trans. JSME, Series B (in Japanese)*, 66-644, pp.186-193, 2000.
- Ref 4 Matsumoto, K., *et al.*, Performance Improvement and Peculiar Behavior of Disk Friction and Leakage in Very Low Specific Speed, *Trans. JSME, Series B (in Japanese)*, 65-640, pp.4027-4032, 1999.
- Ref 5 Kurokawa,J., *et al.*, Performance of a Low Specific Speed Volute Pump , *Turbomachinery (in Japanese)*, 18-5 , pp. 330-338, 1990.
- Ref 6 Choi, Y-D., *et al.*, Internal Flow Characteristics of a Very Low Specific-Speed Semi-Open Impeller, *Turbomachinery (in Japanese)*, 31-1 , pp. 43-52, 2003.
- Ref 7 Choi, Y-D., Kurokawa,J., Matsui,J., Performance and Internal Flow Characteristics of a Very Low Specific Speed Centrifugal Pump, *J. Fluids Eng.*, Vol. 128, pp. 341-348 , 2006.
- Ref 8 Kagawa,S., *et. al*, Performances of Very Low Specific Speed Centrifugal Pump with Circular Casing, *Trans. JSME, Series B (in Japanese)*, 71-707, pp. 1821-1828 , 2005.